Anomalous Hardening Behavior of a Calcium Phosphate Bone Cement

Amanda Generosi,[†] Julietta V. Rau,*[,†] Vladimir S. Komlev,[‡] Valerio Rossi Albertini,[†] Alexandr Yu. Fedotov,[‡] and Sergey M. Barinov[‡]

Istituto di Struttura della Materia, Consiglio Nazionale delle Ricerche, via del Fosso del Cavaliere, 100-00133 Rome, Italy, A.A. Baikov Institute of Metallurgy and Materials Science, Russian Academy of Sciences, Leninsky prospect 49, 119991 Moscow, Russia

Received: July 31, 2009; Revised Manuscript Received: November 5, 2009

In this work, an anomalous microscopic and macroscopic behavior during the hardening process of a calcium phosphate cement, based on anhydrous dicalcium phosphate, was observed. Indeed, the standard compressive strength measurements provided completely unexpected results, which encouraged a deeper investigation by means of X-ray diffraction, Fourier transform infrared spectroscopy, and scanning electron and atomic force microscopies. The energy dispersive X-ray diffraction mode was preferred to the conventional angular dispersive one, the former being particularly suitable for the real-time studies, allowing us to follow the hardening process in situ and to confirm that the investigated cement undergoes a long-time crystallization much more complex than expected. Indeed, the sequence of diffraction patterns exhibited anomalous intensity modulations (corresponding to structural changes taking place upon hardening) being consistent, and even in phase, with the variations of the compressive strength. These anomalous intensity modulations were confirmed also by the in situ time-resolved Fourier transform infrared spectroscopy. The explanation of the anomalous behavior was given by means of a multiscale approach correlating the microscopic (structural) and macroscopic (compressive strength) properties. In perspective, this finding may be interesting not only from the fundamental materials science point of view, but also for novel applications. For example, it might be utilized as an "intrinsic bioreactor", playing the role of stimulator of cellular proliferation by exerting stresses due to its alternative contracting and expanding internal forces on the tissues.

1. Introduction

A number of calcium phosphate cements (CPC) have been developed since the early 1980s.[1,2] They are of great interest for bone tissue repair, owing to their good biocompatibility and easy shaping, for any complex three-dimensional geometry.[3,4] These cements are blends of amorphous and/or crystalline calcium orthophosphate powder(s) that, once mixed with a liquid phase, give a moldable paste. The setting reaction promotes hardening of the paste through entanglements of the crystals in the precipitate.[5]

In this work, we investigated a dicalcium phosphate based cement, that as well as the other calcium orthophosphate cement combinations, is well-known in the literature.[3,6,7] On the other hand, the role of silicates involved in the biomineralization of apatite has long been a subject of much scientific interest for bone cements application.[8−10] Silicon is believed to be essential for skeletal development.[8] It was reported that silicon is localized in the active areas of young bone and is involved in the early stage of bone calcification. More recently, some authors indicated also the potential ability of the silicon-containing bioactive glasses to activate bone-related gene expression and to stimulate cell proliferation.[11−13]

Here, we report an anomalous behavior observed during the hardening process of a cement based on dicalcium phosphate anhydrous (DCPA, monetite) and a sodium silicate solution. The standard compressive strength measurements provided completely unexpected results, which induced a deeper X-ray diffraction investigation. Usually, to detect the initial and final phases of a cement hardening process, common laboratory (angular dispersive) X-ray diffraction studies are performed. However, it was demonstrated that to follow the hardening process in situ, the energy dispersive variant of X-ray diffraction (EDXRD) is much more suitable and reliable, because of some important advantages with respect to its angular dispersive counterpart.[14,15] The hardening−crystallization process is generally described by a sigmoid increase of the grain size over time,[16] the expected characteristic crystallization time being of some hours. After this period, the structure is considered to be essentially stable and only slow secondary processes are expected to take place on a longer time scale, such as possible coalescence of crystal grains and relaxations of internal stresses, eventually resulting in cement consolidation. These processes do not produce dramatic changes in diffraction patterns, being only associated with a slight narrowing and small shifts, respectively, of the reflection peaks.

In the present in situ EDXRD study, we performed a long-term measurement and unexpectedly observed that the investigated cement undergoes a long-time crystallization behavior much more complex than assumed, as witnessed by numerous and remarkable diffraction pattern changes. Furthermore, in situ time-resolved Fourier transform infrared spectroscopy (FTIR) was accomplished confirming the anomalous structural behavior. To complete the investigations, scanning electron microscopy (SEM) and atomic force microscopy (AFM) morphological studies were also performed.

* To whom correspondence should be addressed. Tel: +39-06-4993 4124. Fax: +39-06-4993 4153. E-mail: giulietta.rau@ism.cnr.it.
[†] Istituto di Struttura della Materia.
[‡] Russian Academy of Sciences.

10.1021/jp907350u
Published on Web 12/29/2009

2. Experimental Section

2.1. Materials. Analytical purity-grade calcium dihydrogen phosphate dihydrate ($CaHPO_4 \times 2H_2O$) (Brushite, DCPD) was calcinated in order to convert it into dicalcium phosphate anhydrous ($CaHPO_4$) (Monetite, DCPA) in an air atmosphere furnace at 150 °C for 2 h. Afterward, the DCPA powder was immersed in 95% ethanol for 24 h, and then this mixture was ground in a planetary ball mill to obtain particles of about 1 μm size.

A commercial glass with a nominal composition of 20 mol % Na_2O and 80 mol % SiO_2 was used. It was manufactured by a conventional melting-quenching of a powder mixture of Na_2CO_3 and SiO_2 reagent-grade chemicals. Afterward, a sodium silicate solution ($Na_2O-SiO_2-H_2O$ system) with pH = 8.2, water content of about 50−60%, and with an as-batched silicate modulus of 3 was prepared and used as hardening liquid phase.[17]

To obtain the cement paste, the DCPA powder was intensively mixed with the hardening liquid on a flat laboratory glass, until a dense homogeneous creamy paste was formed (about 2 min). The liquid-to-powder ratio was about 0.25 mL/0.25 g. One part of the so-obtained paste was immediately placed into the diffractometer's sample holder to perform the pattern collection, while the other part was used to measure the compressive strength.

The mixture containing chitosan was prepared adding 0.01 g of water-soluble, low molecular weight (38.2 kDA) chitosan to the hardening liquid followed by an intensive mixing for 1 min until a homogeneous mixture was formed.

2.2. Energy Dispersive X-ray Diffraction Method. In this work, an ED diffractometer was applied.[18] The energy spectrum of the primary beam (55 keV) is produced by a W-anode X-ray tube and, after it is modulated by the interaction with the sample, the resulting diffracted radiation is analyzed by an ultra pure Ge single crystal solid state detector. Although, in EDXRD, the q-resolution is lower, it has important advantages. Indeed, in this case, the experimental geometry is static during data acquisition, no angular movement being necessary.[19] This feature, combined with a much faster data acquisition (the number of photons contained in the white component of the primary beam spectrum is about 2 orders of magnitude higher than the number of photons concentrated in the fluorescence lines), makes the technique particularly suitable for the in situ time-resolved measurements, allowing one to follow the real-time structural changes occurring on time scales varying from a few minutes up to several weeks.

In the case of EDXRD, the data analysis is more complicated than that of ADXRD.[22] Particular care must be devoted to the method for estimating the grain size from the energy dispersive diffraction patterns, because the Scherrer formula, which applies to the angular dispersive case only, must be suitably modified. The procedure, based on the Laue equations, is fully described elsewhere.[16]

2.3. Compressive Strength Measurements. The compressive strength of the DCPA cement was evaluated in accordance with the ISO9917E.[20] The prepared cylindrical samples (about 12 mm height and 6 mm diameter) were measured at different hardening times, from 1 to 60 h (samples number $n = 5$ for each point). Compression testing was carried out using an Instron 4082 (Bucks, UK) testing machine operating at a crosshead speed of 1 mm $\times$ min^{-1}.

2.4. Fourier Transform Infrared Spectroscopy. FTIR analysis was carried out collecting a sequence of spectra by means of a Jasco FT/IR 470 Plus interferometer (Italy) equipped with an IRTRON IRT-30 microscope. Each spectrum was acquired in the transmittance mode by executing 250 scans at 8 cm^{-1} resolution. The spectra were collected on the same portion of the DCPA cement paste (in situ) every hour starting from the eighth hour after the sample preparation and for a total of 62 h of hardening time.

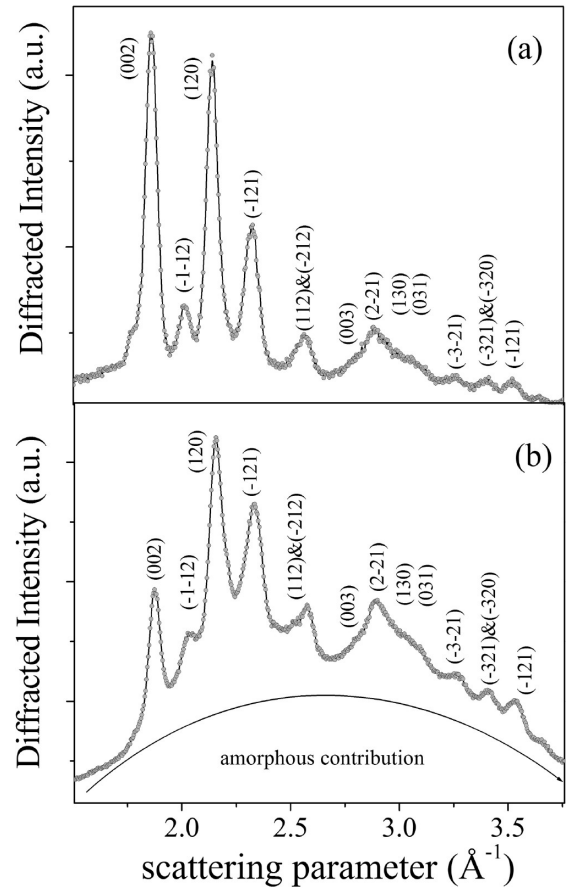

Figure 1. (a) EDXRD pattern collected from the DCPA powder (peaks are labeled) as a function of the scattering parameter. (b) EDXRD pattern collected under the same experimental conditions as in panel a, collected from the final cement after 60 h of hardening.

2.5. Microscopy Measurements. Scanning electron microscopy (a LEO 1420 variable pressure apparatus (Germany)), working in secondary and backscattered electron modes, was used for morphological studies of the investigated cement starting from the fifth hour after the sample preparation, and for a total of 70 h of hardening time. The resolution of the apparatus in vacuum conditions was about 4 nm.

Furthermore, atomic force microscopy measurements were performed in a noncontact mode using a homemade air-operating microscope,[21] to quantitatively evaluate the surface texture, roughness, and the aggregate dimensions.

3. Results and Discussion

EDXRD measurements were performed on both the DCPA powder and the final cement, to obtain their accurate structural characterization and comparison, as shown in Figure 1 panels a and b, respectively. The patterns, plotted as a function of the scattering parameter, were both collected in transmission geometry, and the experimental conditions were kept unchanged during the whole acquisition: the scattering angle 2ϑ was set at 9.0°, the voltage power supply was set at 55 kV (corresponding to a maximum energy of the white spectral component of 55 keV) and the optical path was defined by three square collimation slits, their aperture being (300 $\times$ 300) μm.

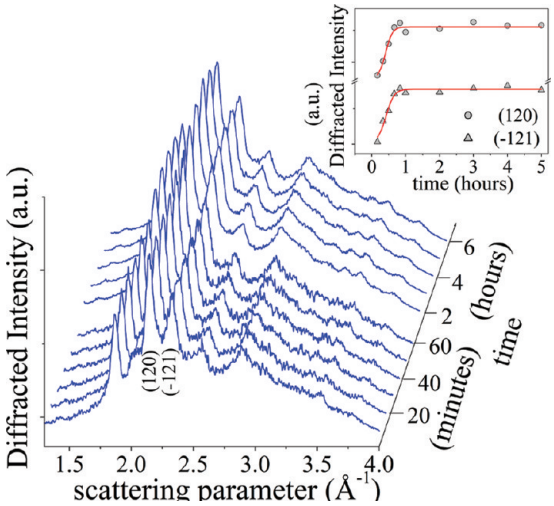

Figure 2. Sequence of EDXRD patterns collected as a function of the scattering parameter and of time (short-time scale) during the hardening of the DCPA cement. In the inset, the time evolution of the (120) and ($\bar{1}$21) reflections intensity (dots and triangles, respectively), showing the kinetics of the primary crystallization of the DCPA cement, is reported.

Both spectra (Figure 1) perfectly fit a triclinic monetite powder diffraction pattern, space group $P\bar{1}(2)$ (card number 75-1520[22]), and all the reflections detected in the explored q-range can be easily assigned. However, a few differences can be noticed by a first qualitative evaluation of the DCPA powder and the cement diffraction patterns. In Figure 1a, the proportions among the Bragg reflections are in good agreement with the relative intensities attributed in the literature[22] to the DCPA powder, that is, 100% of the (002) reflection intensity and 80% of the (120) one, for example. Instead, in Figure 1b, these relative intensity ratios are not preserved, indicating that the crystallization process may not occur homogeneously along all the crystallographic directions. Moreover, the final cement pattern shows a diffuse scattering component (bump underlying the crystalline reflections) that can be attributed to both the liquid component used as hardening agent and to the presence of nanocrystalline (and, therefore, X-ray amorphous) grains. This hypothesis is also supported by the fact that the crystalline Bragg peaks are broader in Figure 1b, compared to the powder diffraction pattern reflections in Figure 1a. This indicates that the crystalline grains formed during the hardening process are smaller than those of the pristine $CaHPO_4$ powder domains.

In our previous works,[14,15] it was demonstrated that the hardening mechanism of calcium phosphate bone cements typically consists of a primary crystallization (peak intensity growth), occurring in a characteristic time of minutes, and a subsequent secondary crystallization, that is, the growth of the crystalline grain dimensions, occurring on a much longer time scale (hours).[16] In this work, in order to study the hardening process of the DCPA cement, in situ time-resolved EDXRD measurements were performed collecting patterns every 10 min during the first hour of acquisition and, then, every half an hour up to 6 h of the overall structural monitoring. In Figure 2, the sequence of the so-obtained diffraction patterns is shown, the crystallographic assignment being the same of Figure 1b. The quantitative analysis of the peak intensities variation of the subsequent patterns allowed the monitoring of the primary crystallization, which occurs isotropically in a characteristic time of $\tau = (25 \pm 2)$ minutes. In the inset of Figure 2, the time evolution of the (120) and ($\bar{1}$21) reflections during the primary crystallization is shown, the other peaks following similar trends.

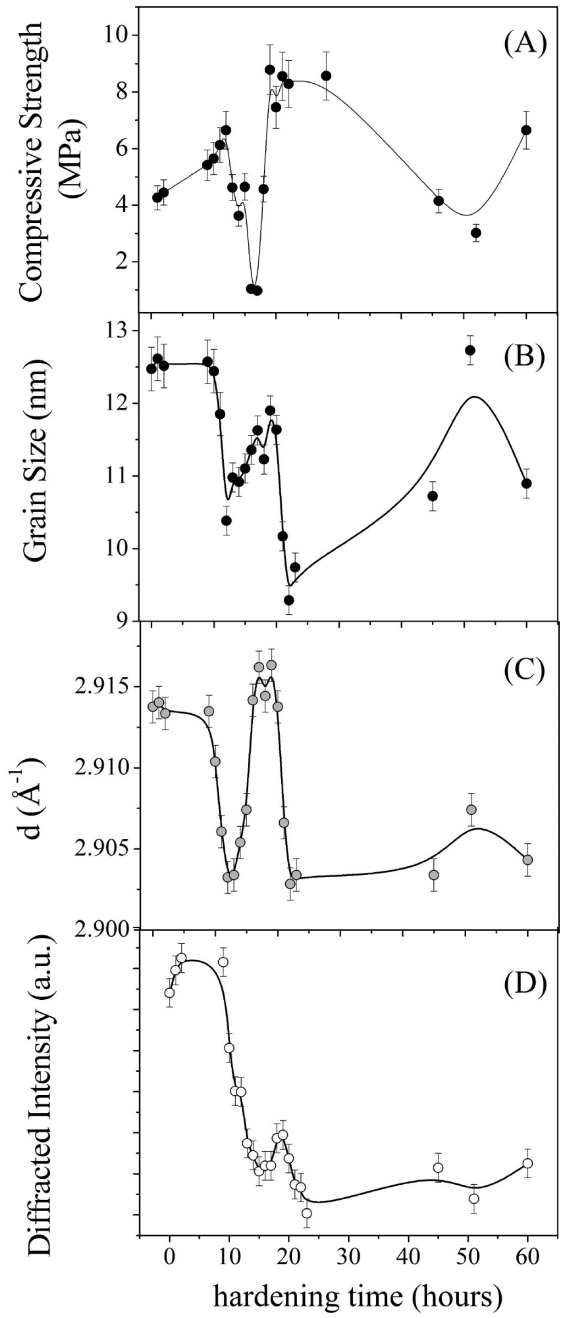

Figure 3. Mechanical and structural variations as a function of the hardening time of the DCPA cement: (A) compressive strength, (B) crystalline (120) grain dimension, (C) (120) interplanar spacing, (D) (120) relative intensity.

No evidence of the further crystal domain growth was found, that is, no variation of the full width half maximum (fwhm) of the peaks was observed after they had reached their maximum intensity (in about 1 hour, as shown in the inset of Figure 2). In fact, the nanometric size of the crystalline phases deduced from the fwhm of the peaks was found (by applying the Scherrer equation) to be preserved, during the primary crystallization process. It ranges from 10 to 15 nm, depending on the reflection on which the Scherrer analysis was performed.

Subsequently, the mechanical properties of the DCPA cement were measured. The obtained results are presented in Figure 3A. Usually, the compressive strength behavior is described by an initial sigmoidal growth followed by a plateau, indicating the saturation. In this case, a completely anomalous mechanical behavior of DCPA cement was detected, characterized by a

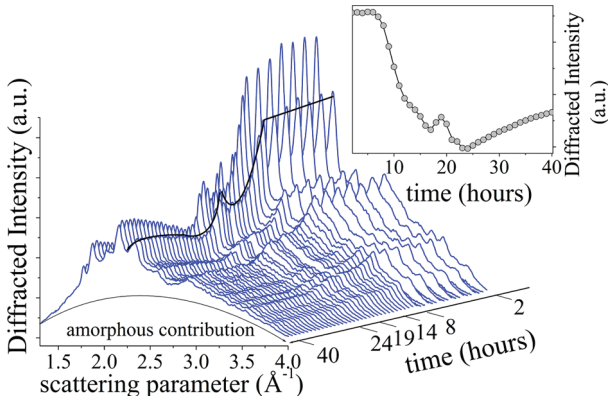

Figure 4. Sequence of EDXRD patterns collected as a function of the scattering parameter and of time (long-time scale) during the hardening of the DCPA cement. In the inset, the overall diffraction intensity variation is reported as a function of the hardening time.

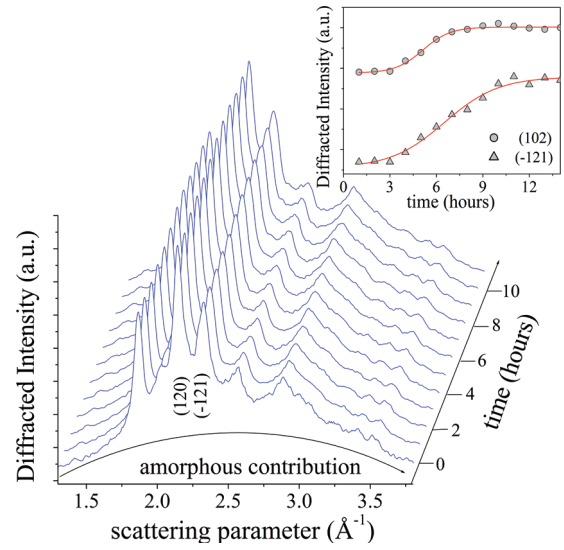

Figure 5. Sequence of EDXRD patterns, collected as a function of the scattering parameter and of time (short-time scale), during the hardening of the DCPA cement with the addition of chitosan. In the inset, the time evolution of the (120) and ($\bar{1}$21) reflection intensities (dots and triangles, respectively), showing the kinetics of the primary crystallization of the DCPA cement, is reported.

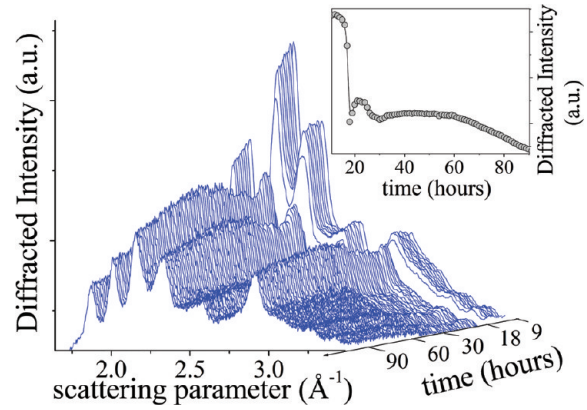

Figure 6. Sequence of EDXRD patterns, collected as a function of the scattering parameter and of time (long-time scale) during the hardening of the DCPA cement with the addition of chitosan. In the inset, the overall diffraction intensity variation is reported as a function of the hardening time.

sequence of peaks and valleys on the compressive strength curve observed during the hardening process. The first maximum and minimum can be easily explained. It is known that the hydration process of a CPC is controlled by the dissolution and precipitation of the initial calcium phosphates,[23] these latter processes being connected to the degree of supersaturation or undersaturation of the corresponding solutions. However, the other extremums on the compressive strength curve are not clear.

To understand the origin of the anomalous mechanical properties evidenced upon the hardening time, another set of in situ time-resolved EDXRD measurements was performed, the patterns being collected every hour for an overall acquisition time of 60 h. In fact, it is well-known that the structural and mechanical behaviors are closely related and that structural modifications could be induced by a macroscopic mechanical variation.

In Figure 4, the sequence of diffraction patterns is plotted as a function of both the scattering parameter and the hardening time. Even at a first qualitative evaluation, a very unusual intensity change over time can be immediately noticed, as shown in Figure 4 by a black line, which evidence that the diffracted intensity exhibits a strong modulation during the hardening process. This trend was quantified calculating the variation of the overall diffracted intensity as a function of time and the result is reported in the inset of Figure 4, being perfectly consistent with the preliminary observations. Possible instrumental and experimental reasons of why this effect was accurately analyzed and excluded include (1) no primary beam intensity fluctuations upon the pattern collection period were registered; (2) no sample misalignment occurred upon measurements; (3) no collimation slit displacement took place.

However, the most important demonstration that this is not an artifact is that the same effect (i.e., significant modulation of the diffracted intensities) was detected on the cement sample prepared by adding chitosan to the initial cement paste. Indeed, chitosan is known to slow down the hardening process of calcium phosphate bone cements, inducing sterical constraints in the structural reorganization of cement.[15] A novel paste containing chitosan was prepared and in situ time-resolved EDXRD measurements were performed under the same experimental conditions as reported above, the overall data collection lasting 95 h. In Figure 5, the sequence of EDXRD patterns collected during the first 10 h of hardening is reported, no intensity modulations being detected. In fact, the primary crystallization observed in Figure 2 now occurs on longer time scales, as expected, due to the presence of chitosan. The characteristic time of the process, $\tau = (5.5 \pm 0.5)$ hours, was deduced by the accurate Gaussian fit of the (102) and ($\bar{1}$21) reflections, being representative of the overall hardening process, reported in the inset of Figure 5. The subsequent 85 h of hardening were monitored by collecting a sequence of EDXRD patterns. Despite much longer time scale, the previously described anomalous diffracted intensity behavior was observed again, as shown in Figure 6. In the inset of Figure 6, the intensity variations, calculated as the integral of the overall pattern, are reported as a function of time, exhibiting the same modulation.

This experimental fact confirms that the observed anomalous diffracted intensity behavior corresponds to actual structural changes, taking place upon the hardening process of the DCPA cement. To quantify the structural modifications, the Gaussian analysis of all the reflections of each pattern (Figure 2) was performed, and the following information was deduced: (1) the time evolution of the position of each reflection, related to the variations of the lattice parameters; (2) the time evolution of the fwhm of each reflection, related to the variation of the crystalline grain size, through the Sherrer formula; (3) the time

evolution of the reflections intensity, related to the number and average size of grains, whose lattice planes are perpendicular to the scattering vector. The results of this analysis are reported in Figure 3panels, B, C, and D, respectively, being perfectly consistent with each other and in good agreement with the compressive strength measurements. Indeed, the compressive strength of the DCPA cement changes upon the hardening time, as shown in Figure 3A, having 1 order of magnitude excursion (from 1 to 10 MPa). Two modulations can be clearly observed, the first having a period of $\tau_1 = (7 \pm 1)$ h and the second a period of $\tau_2 = (33 \pm 1)$ h. As visible in Figure 3, the structural transformations of this material follow the same modulation trend and have the same characteristic times of the mechanical property changes. The microscopic phenomena taking place in the system can be described in the following way: as the compressive strength increases, inducing a stress into the ordered crystalline structure, the lattice contracts inducing a peak shift toward the higher q values (lower d values, Figure 3C). This stress can be quantified in terms of the relative shift from the original peak positions (corresponding to the unstressed lattice parameters) and amounts to about 0.5%. Moreover, as the lattice parameters vary accordingly to the compressive strength, the crystalline grain size changes too (Figure 3B). Indeed, the stress induced onto the crystalline lattice also effects the grain size, inducing the grains breaking. The grain size diminishes when the lattice is stressed (minimum grain size = 9 nm) and grows, due to the secondary crystallization, when the lattice parameters approach the theoretical unstressed values, reaching a maximum grain size of 12.5 nm, comparable with that of the pristine DCPA paste (hardening time = 0 h). In fact, the crystalline phase dimensions are in the nanometric range during the entire process.

Finally, as a consequence of the grain size variation, the overall diffracted intensity diminishes still modulating with the same characteristic times, as previously reported. Moreover, it is worth noticing that the period of this modulating behavior, is not constant, becoming longer as the structural/mechanical modulation mechanism goes on, likely reaching an asymptotic value on much longer time scales than those monitored in this experimental work. Furthermore, the lattice parameters do not achieve the original unstressed values after the first cycle, which might suggest that the cement structure is not completely elastic. Indeed, the stress−strain curves, being the graphical representation of the relationship between the load applied on the sample and the deformation of the sample, were calculated for different hardening times corresponding to $t_1 = 14$, $t_2 = 25$, and $t_3 = 35$ h. The Young modulus was determined from the slope of these stress−strain curves created during tensile tests conducted on a sample of the material, corresponding to 1.26 (t_1), to 1.35 (t_2) and 2.60 MPa (t_3), respectively. Moreover the rupture point was determined for the above-mentioned samples, occurring when a 23.3% deformation (t_1), a 19.1% deformation (t_2), and a 17.2% deformation (t_3) were reached.

To fully describe the investigated system, in situ time-resolved FTIR study was performed to check if there exists a correspondence between the observed structural/mechanical rearrangements and the vibrational properties of the DCPA molecule. In Figure 7 A, a sequence of FTIR spectra collected as a function of the hardening time is shown. There it can be seen that the intensity variations occur for all the absorption bands. The band around 1751 cm^{-1} can be attributed to the C═O bond stretching. The two broad bands ranging from 1250 to 985 cm^{-1} and from 870 to 780 cm^{-1}, can be attributed to the P−O symmetric and asymmetric stretching and to the P−O−H stretching of the inorganic Ca−P component, respectively, in

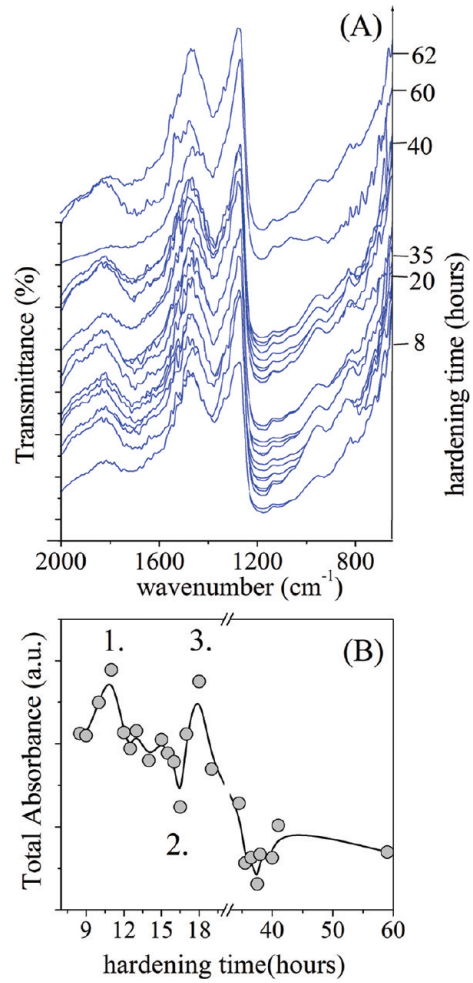

Figure 7. (A) Sequence of FTIR transmittance spectra collected as a function of the hardening time upon the DCPA cement; (B) quantitative evaluation of the total peak area.

agreement with literature data.[24,25] However, in the 1300−740 cm^{-1} region sodium silicate gels are also IR active, showing the two maxima in our range of interest at 1050−1000 cm^{-1} and at 800−750 cm^{-1}, the absorption bands being related to the Si−O−Si bond vibrational modes.[26] Moreover, the amorphous character of the silicate phase contributes to the broadening of the bands resulting in a nonunivocal attribution. Quantitative evaluation of the total peak area in the 2000−750 cm^{-1} range was obtained by an accurate fitting procedure, and the results reported in Figure 8B are representative of the modulating behavior of all the IR bands in this region. As evidenced in Figure 8B (points 1 and 3), the absorption bands intensity reaches two maxima corresponding exactly to the first and second grain size breakdown (and compressive strength maxima), while in point 2 the absorption bands intensity reaches a minimum compatible with the secondary crystallization, that is, the grain size growth. These effects are not unexpected since the existence of smaller crystals enhances the grain surface area, inducing increased IR activity (change in the dipole moment occurring on the grain boundaries).[27] Therefore, also the results of the FTIR measurements confirm the hypothesis proposed above.

Finally, SEM images were collected for morphological characterization of the evolving system, since this technique has been proved to be useful to study the growth mechanism of analogous calcium phosphate materials.[28] In Figure 8, a selection of images representing the evolution of the surface

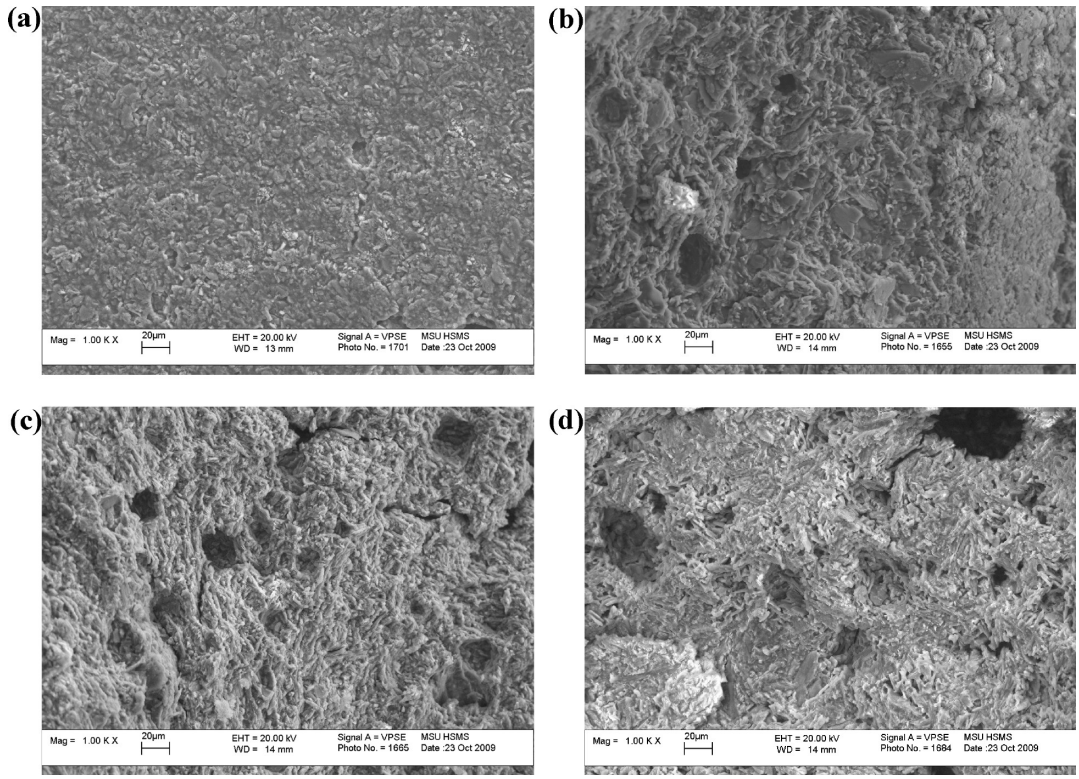

Figure 8. SEM micrographs of the DCPA cement at 1000 magnification: (A) after 5 h of hardening; (B) after 18 h; (C) after 24 h; (D) after 70 h.

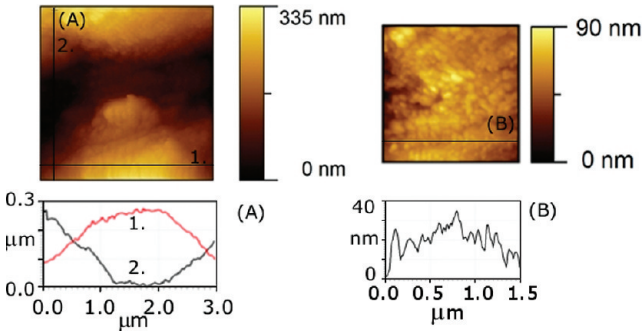

Figure 9. AFM images collected upon the DCPA cement after 85 h of hardening: (A) 3 μm × 3 μm image plotted together with two line profiles collected in correspondence of point 1 and 2; (B) 1.5 μm × 1.5 μm zoom of image A plotted together with a line profile.

morphology of the DCPA cement, as a function of the hardening time, is shown. As can be seen, the initially smooth, compact, and homogeneous structure (A, 5 h of hardening), gradually evolves into structure B (18 h), where it coexists (right side of the image) with a porous, stack-plate crystals agglomerated surface (left side of the image). As the hardening time passes, the initially almost flat and compact morphology turns into a porous texture (C, 24 h). The pores get larger and deeper passing from structure C (24 h) to structure D (70 h), reaching a size up to 30 μm.

AFM topographies were also collected upon the cement after 85 h of hardening (Figure 9). Indeed, the micrometric grains evidenced by SEM are hardly detectable by the AFM microscope due to the limited scanner excursion, being 30 μm along the x and y directions and 3.6 μm along z. However, some interesting information could be deduced by AFM, too, as shown in Figure 9A, where a 3 μm × 3 μm image that evidence the boundary between two adjacent grains is plotted. The horizontal and vertical line profiles are extracted in correspondence of points 1 and 2. They evidence the grain shape (width >3 μm and height >300 nm) and the peak to valley excursion (300 nm). Furthermore, along with large size granular structures (Figure 9A), a nanometric fine texture could be detected in (Figure 9B), where a high resolution 1.5 μm × 1.5 μm image is shown, collected upon the surface of a single grain. As clearly evidenced by the horizontal line profile extracted in correspondence of image B, a nanometric globular fine texture is superimposed to larger grains, the characteristic dimensions of these smaller structures being 100 nm in width and from 10 to 20 nm in height.

Finally, to conclude the characterization of the sample, the density and open porosity of the final product was measured by the common hydrostatic weighing procedure in distillated water. The cement's density was in the range of 2.1−2.5 g/cm^3 and open pores content was from 7 to 12%.

As to the interactions in the investigated system, they could be quite complicated; however, some considerations can be proposed. These interactions, likely, include the formation of dicalcium phosphate dihydrate by combining two water molecules with DCPA. The metastability of the latter leads to the hydrolysis in neutral solution and to the formation of a more basic calcium phosphate, that is, to amorphous phosphate (ACP), which is metastable itself. Silicate groups from the sodium glass solution can inter into ACP and DCPA structures partially substituting the phosphate groups. This is supposed to increase the glass-forming ability, since silica is the best glass forming anion. Sodium can replace partially calcium ions, increasing the charge misbalance in ACP and generally leading to further disordering of the structure.

Regarding the role of the sodium silicate solution, it has been reported that even a simple Na_2O-SiO_2 glass is able to form the Si−OH groups, thereby inducing mineralization of apatite in the simulated body fluid (SBF).[29] While this glass has a simple composition free of calcium and phosphate ions, apatite forma-

tion on its surface was observed to be very sluggish *in vitro*,[30,31] which may be highly beneficial to trace out the surface changes involved in apatite formation. In ref 30 the mechanism of biomineralization of apatite on a Na_2O-SiO_2 glass was investigated *in vitro*, in which the glass surface was surveyed by transmission electron microscopy and energy-dispersive X-ray spectrometry as a function of soaking time in the SBF. The glass was found to exchange Na^+ ions with H_3O^+ ions in the SBF to form silanol (Si−OH) groups on its surface at an early stage of soaking. Immediately after they were formed, the Si−OH groups incorporated calcium ions in the fluid to form an amorphous calcium silicate. After a long soaking time, the calcium silicate incorporated phosphate ions and further calcium ions in the fluid to form an amorphous calcium phosphate with a low Ca/P atomic % ratio (1.43). The amorphous calcium phosphate was eventually converted into crystalline apatite, which contained small amounts of Na, Mg, and Cl and had a Ca/P ratio of 1.65, similar to that of the bone mineral.

In prospective, the finding described in this work may be interesting not only from the fundamental materials science point of view, but could be also potentially useful for novel applications. In particular, it could be extrapolated to different biomedical research areas, for example, utilized as a new approach to the so-called "in situ tissue regeneration", which involves biomaterials in combination with drugs or external force-specific effects to stimulate the local tissue repair, thus activating the cells response that, in turn, are induced to self-assemble into the required tissues in situ.[32] It is known that cells and tissues react to external mechanical stimuli that can include gravitational and hydrostatic pressures, shear stresses caused by fluid flow, acoustic waves, and contractile forces transmitted from one cell to another. A large number of studies have demonstrated that the biological environment of tissues is highly influenced by the mechanical forces applied to the cells. Therefore, ideally, to mime the physiological environment, similar conditions should be reproduced *in vitro* during the cell culture. Such conditions can be obtained in a suitable bioreactor, by applying an external force-specific effect.[33−37] A further step might be the design of materials exhibiting special properties, that is to say a natural bioreactor that plays the role of an intrinsic stimulator of cellular proliferation by exerting stresses and contracting internal forces on the tissues, thus making the application of an external force to stimulate the cell growth, unnecessary.

Further studies of the biocompatibility of the DCPA cement are in progress.

4. Conclusions

New interesting properties of the DCPA cement were discovered. Anomalous and unexpected hardening behavior was observed during the compressive strength measurements. This behavior was further confirmed by means of a diffraction technique particularly suitable for this purpose, the EDXRD, and accurately described by the pattern analysis, in terms of crystal growth, followed by a break down to the nanometric size domains. This effect can be controlled by the chitosan addition.

The explanation of this finding is provided by means of a multiscale approach, correlating the microscopic and macroscopic properties: time-resolved structural data obtained upon cements hardening by the in situ EDXRD (the grains size evolution) and the in situ FTIR, and the compressive strength measurements. Additional morphological information on the investigated cement was provided by the SEM and AFM techniques.

Acknowledgment. Authors are grateful to the Russian Foundation for Basic Research (RFBR), Grant No. 09-03-00187a, for the partial financial support. V.S. Komlev thanks the President of the Russian Federation for financial support (Grant No. MK 4047.2008.3 for "Young Russian Scientists"). The authors thank Dr. Stella Nunziante Cesaro for interesting and helpful discussion regarding the FTIR results.

References and Notes

(1) LeGeros, R. Z.; Chohayeb, A.; Shulman, A. *J. Dent. Res.* **1982**, *61*, 343.
(2) Brown, W. E.; Chow, L. C. *J. Dent. Res.* **1983**, *62*, 672.
(3) Dorozhkin, S. V. *Materials* **2009**, *2*, 221–291.
(4) Dorozhkin, S. V. *Materials* **2009**, *2*, 399–498.
(5) Wang, X.; Ye, J.; Wang, Y. *J. Mater. Sci.: Mater. Med.* **2008**, *19*, 813–816.
(6) Burguera, E. F.; Xu, H. H. K.; Weir, M. D. *J. Biomed. Mater. Res., B* **2006**, *77*, 126–134.
(7) Burguera, E. F.; Guitian, F.; Chow, L. C. *J. Biomed. Mater. Res., A* **2004**, *71*, 275–282.
(8) Wang, X.; Ye, J.; Wang, Y. Chen. *J. Biomed. Mater. Res., B* **2007**, *82B*, 93–99.
(9) Huan, Z.; Chang, J. *J. Biomed. Mater. Res., B* **2007**, *82B*, 352–359.
(10) Huan, Z.; Chang, J. *J. Mater. Sci. Mater. Med.* **2009**, *20*, 833–841.
(11) Hench, L. L.; West, J. K. *Life Chem. Rep.* **1996**, *13*, 187–241.
(12) Xynos, I. D.; Edgar, A. J.; Buttery, L. D. K.; Hench, L. L. M.; Polak, J. M. *J. Biomed. Mater. Res., A* **2001**, *55*, 151–157.
(13) Gough, J. E.; Jones, J. R.; Hench, L. L. *Biomaterials* **2004**, *25*, 2039–2046.
(14) Generosi, A.; Smirnov, V. V.; Rau, J. V.; Rossi Albertini, V.; Ferro, D.; Barinov, S. M. *Mater. Res. Bull.* **2008**, *43*, 561–571.
(15) Rau, J. V.; Generosi, A.; Smirnov, V. V.; Ferro, D.; Rossi Albertini, V.; Barinov, S. M. *Acta Biomater.* **2008**, *4*, 1089–1094.
(16) Smirnov, V. V.; Rau, J. V.; Generosi, A.; Rossi Albertini, V.; Ferro, D.; Barinov, S. M. *J. Biomed. Mater. Res., B*, DOI: 10.1002/jbm.b.31560, available online December 18, 2009.
(17) Orlov, Y. I. *Glass. Phys. Chem.* **2002**, *28*, 281–287.
(18) Felici, R.; Cilloco, F.; Caminiti, R.; Sadun, C.; Rossi, V. It Patent, RM 93 A 000410, 1993.
(19) Caminiti, R.; Rossi Albertini, V. *Int. Rev. Phys. Chem.* **1999**, *18*, 263–299.
(20) *ISO 9917 Specification for Dental Water-Based Cements*; International Organization for Standardization: Geneva, 1994.
(21) Cricenti, A.; Generosi, R. *Rev. Sci. Instrum.* **1995**, *66*, 2843–2847.
(22) *Database JCPDS 2000*; International Centre for Diffraction Data: Newtown Square, PA, 2000.
(23) Fernandez, E.; Gil, F. J.; Ginebra, M. P.; Driessens, F. C. M.; Plannel, J. A.; Best, S. M. *J. Mater. Sci.: Mater. Med.* **1999**, *10*, 223–230.
(24) Tortet, L.; Gavarri, J. R.; Nihoul, G.; Dianoux, A. J. *J. Solid State Chem.* **1997**, *132*, 6–16.
(25) Zhou, S.; Su, Q.; Li, X.; Weng, J. *Mater. Sci. Eng., A* **2006**, *430*, 341–345.
(26) Dimas, D.; Giannopoulou, I.; Panias, D. *J. Mater. Sci.* **2009**, *44*, 3719–3730.
(27) Griffiths, P.; De Haseth, J. A. *Fourier Transform Infrared Spectrometry;* Chemical Analysis: A Series of Monographs on Analytical Chemistry and Its Applications; John Wiley & Sons. Inc.: Hoboken, New Jersey, 2007.
(28) Rodríguez-Lugo, V.; Sanchez Hernández, J.; Arellano-Jimenez, Ma. J.; Hernández-Tejeda, P. H.; Recillas-Gispert, S. *Microsc. Microanal.* **2005**, *11*, 516–523.
(29) Kim, H.-M.; Miyaji, F.; Kokubo, T.; Ohtsuki, C.; Nakamura, T. *J. Am. Ceram. Soc.* **1995**, *78* (9), 2405–11.
(30) Hayakawa, S.; Tsuru, K.; Ohtsuki, C.; Osaka, A. *J. Am. Ceram. Soc.* **1999**, *82*, 2155–2160.
(31) Takadama, H.; Kim, H.-M.; Kokubo, T.; Nakamura, T. *Chem. Mater.* **2001**, *13*, 1108–1113.
(32) Hench, L. L.; Polak, J. M. *Science* **2002**, *295*, 1015–1017.
(33) Janmey, P. A.; Weitz, D. A. *Trends Biochem. Sci.* **2004**, *29*, 364–370.
(34) Martin, I.; Wendt, D.; Heberer, M. *Trends Biotechnol.* **2004**, *22*, 80–86.
(35) Salgado, A. J.; Coutinho, O. P.; Reis, R. L. *Marcomol. Biosci.* **2004**, *4*, 743–765.
(36) Sikavitsas, V. I.; Temenoff, J. S.; Mikos, A. G. *Biomaterials* **2001**, *22*, 2581–2593.
(37) Mano, J. F.; Reis, R. L. *J. Tissue Eng. Regen. Med.* **2007**, *1*, 261–273.

JP907350U